Monatshefte für Chemie 129, 1119–1132 (1998)

Monatshefte für Chemie
Chemical Monthly

New Insights into the Solvent Effect on the Electrooxidation Kinetics of Nickelocene

Krzysztof Winkler

Institute of Chemistry, University of Bialystok, PL-15443 Bialystok, Poland

Summary. The kinetics of the one-electron oxidation of nickelocene are studied by ac-voltammetry in different aprotic solvents at mercury and platinum ultramicroelectrodes. A double layer correction has been applied to the reported electron transfer rate constants. The influence of solvent on the activation enthalpy is also examined. Solvent effects on the electron transfer rate constants and activation enthalpies are interpreted within the context of the encounter-pre-equilibrium model. Several different methods are used to analyse the solvent effect on the kinetics of nickelocene oxidation. The parameters of the charge transfer process (the equilibrium constant for the precursor complex formation) are obtained on the basis of these analyses.

Keywords. Nickelocene electrooxidation; Kinetics of charge transfer; Solvent effect on electron transfer.

Neue Ergebnisse zum Einfluß des Lösungsmittels auf die Kinetik der Elektrooxidation von Nickelocen

Zusammenfassung. Die Kinetik der Einelektronenoxidation von Nickelocen an Quecksilber- und Platinultramikroelektroden wurde in verschiedenen aprotischen Lösungsmitteln mit Hilfe von AC-Voltammetrie untersucht. Die angegebenen Geschwindigkeitskonstanten des Elektronenübergangs wurden unter Anwendung einer Doppelschichtkorrektur erhalten. Der Einfluß des Lösungsmittels auf die Aktivierungsenthalpie wurde ebenfalls untersucht. Die Lösungsmitteleinflüsse werden im Sinn des *encounter-pre-equilibrium*-Modells interpretiert. Zur Untersuchung des Lösungsmitteleffekts auf die Oxidation von Nickelocen wurden verschiedene Methoden eingesetzt, die eine Berechnung der Parameter des *charge-transfer*-Prozesses (d.h. der Gleichgewichtskonstante der Bildung des Vorläuferkomplexes) erlauben.

Introduction

The influence of structural and thermodynamic factors on electron transfer reactions is the subject of extensive current debate [1–4]. It is now generally recognized that the solvent can affect the magnitude of the *Gibbs* activation energy (ΔG^*) and the pre-exponential factor (A). For a fast charge transfer process, the standard rate constant can be expressed by Eq. (1) where κ is the electronic transition coefficient, K_p is the equilibrium constant for the formation of the precursor complex, τ_L is the longitudinal relaxation time, Θ is a fraction between 0

and 1 describing the degree of reaction adiabacity, and ΔG_{is}^{*} and ΔG_{os}^{*} are the inner- and outer-sphere reorganization energies, respectively.

$$K_s = \kappa K_p \left(\frac{\Delta G_{os}^{*}}{4\pi RT}\right)^{1/2} \cdot \tau_L^{-\Theta} \cdot \exp\left(-\frac{(\Delta G_{os}^{*} + \Delta G_{is}^{*})}{RT}\right) \tag{1}$$

Recently, it has been shown [5] that the outer-sphere *Gibbs* reorganization energy can be described successfully within the context of the mean spherical approximation (MSA) model by Eq. (2) where a is the radius of the reactant, ε_{op} and ε_s are the optical and static dielectric constants, respectively, ε_o is the vacuum permittivity, and δ_s is the MSA parameter.

$$\Delta G_{os}^{*} = \frac{N_o e^2}{32\pi\varepsilon_o a}\left(\left(1 - \frac{1}{\varepsilon_{op}}\right) - \left(1 - \frac{1}{\varepsilon_s}\right)\frac{1}{1 + \frac{\delta_s}{a}}\right) \tag{2}$$

Eq. (1) shows that the rate of electron transfer depends on the longitudinal relaxation time. However, if the relaxation of solvent molecules is very fast ($\tau_L < 10^{-12}$ s), the rate of precursor complex formation may be limited by the solvent interial effect [6, 7, 9]. In the case of polar solvents, Eq. (3) is valid for the pre-exponential factor [9]; τ_r is the solvent rotational time which depends on the moment of interia of the solvent molecule (I) according to Eq. (4). The ϕ parameter in Eq. (3) can be expressed as given in Eq. (5) where ρ is the molar density and μ is the effective dipole moment.

$$A = \kappa K_p \cdot \sqrt{\frac{2\varepsilon_s \phi}{2\pi\tau_r}} \tag{3}$$

$$\tau_r = \sqrt{\frac{I}{k_B T}} \tag{4}$$

$$\phi = \frac{4\pi\rho\mu^2}{3\,k_B T} \cdot \frac{1}{\varepsilon_s - 1} \tag{5}$$

When the frequency factor depends both on τ_L and τ_r, Eq. (6) holds where $c = \sqrt{\frac{RT}{\pi\Delta G_{os}^{*}}}$.

$$A = \frac{\kappa K_p}{2\pi c\tau_L}\left(\frac{1}{2} + \frac{1}{2}\left(1 + \frac{2\tau_r^2}{c^2\varepsilon_s\phi\tau_L^2}\right)^{1/2}\right)^{-1} \tag{6}$$

The activation parameters of the charge transfer process are also affected by the dynamic properties of the solvent [2, 3]. For an adiabatic reaction, the activation enthalpy (ΔH_{ex}^{*}) is given by Eq. (7) where ΔH_{os}^{*} and ΔH_{is}^{*} are the true outer- and inner-sphere activation enthalpies. The $\partial \ln A/\partial(1/T)$ term can be expressed by Eq. (8) [8].

$$\Delta H_{ex}^{*} = \frac{\partial \ln k_s}{\partial(T^{-1})} = \frac{\partial \ln A}{\partial(T^{-1})} + \Delta H_{os}^{*} + \Delta H_{is}^{*} \tag{7}$$

$$\frac{\partial \ln A}{\partial(T^{-1})} = \frac{\partial \ln \tau_L^{\Theta}}{\partial(T^{-1})} - \frac{RT}{2} \cdot \frac{\Delta G_{os}^{*}}{\Delta H_{os}^{*}} \tag{8}$$

Three general approaches may be used to analyze the solvent effect on the kinetics of fast charge transfer processes:

(*i*) The experimentally obtained standard rate constants can be analyzed as a function of dynamic and energetic factors ($\ln k_s$ as a function of $\ln \tau_L$ [9–19] or $\ln \eta$ [10, 20–22]). The first of these relations is given by Eq. (1). The relationship between viscosity and the *Debye* relaxation time τ_D indicates that the rate of the electrode process should also correlate with viscosity [23]. For these two correlations, the effect of the thermodynamic factor (ΔG^*) is neglected in considering the solvent effect. A more sophisticated analysis taking into account both dynamic and energetic factors is based on the linear relationship between $\ln(k_s \tau_L^{\Theta}/\gamma^{1/2})$ and γ (where $\gamma = 1/\varepsilon_{op} - 1/\varepsilon_s$). This type of analysis yields values for the κK_p parameter. In the systems studied so far, rather poor correlations between $\ln(k_s \tau_L^{\Theta}/\gamma^{1/2})$ and γ have been found [24, 25]. *Weaver* [11] has proposed a somewhat different thermodynamic approach in which Eq. (1) can be rewritten as

$$\ln \frac{k_s}{(\Delta G_{os}^*)^{1/2}} + \frac{\Delta G_{os}^*}{RT} = \ln \left(\frac{\kappa K_p}{(4\pi RT)^{1/2}} \right) - \frac{\Delta G_{is}^*}{RT} + \Theta \ln \tau_L \qquad (9)$$

This equation demonstrates that there should be a linear relationship between the function on the left hand side and $\ln \tau_L$ with a slope equal to Θ.

(*ii*) Eq. (7) and (8) predict that there should be a correlation between experimental activation enthalpy (ΔH_{ex}^*) and longitudinal relaxation enthalpy ($\Delta H_L = \mathrm{d}(\ln \tau_L)/\mathrm{d}(1/T)$) or diffusion enthalpy (ΔH_D). The Θ parameter can be obtained from the slope of the linear relationship between ΔH_{ex}^* and ΔH_L or ΔH_D. However, this kind of analysis is rather controversial [26]. Longitudinal relaxation time is given by Eq. (10) where τ_D is the *Debye* relaxation time and ε_∞ is the dielectric constant of the solvent at infrared frequencies. The temperature dependence of ε_s is well known, but no reliable data for the temperature dependence of ε_∞ and τ_D exist in the current literature [26]. Therefore, the H_D values are often dubious. Another approach is an analysis of the true other-sphere activation enthalpy as a function of γ.

$$\tau_L = \left(\frac{\varepsilon_\infty}{\varepsilon_s} \right) \tau_D \qquad (10)$$

(*iii*) The third approach to solvent effect analysis is based on a comparison of the experimentally obtained kinetic or activation parameters of the charge transfer process with theoretically predicted values.

In this paper, the results of a study into the solvent effect on the process of nickelocene ($Ni(Cp)_2$) oxidation are presented. A combination of ac-voltammetric techniques employing ultramicroelectrodes has made possible the acquisition of reliable data [27, 28]. The rate of the electrode reaction was additionally corrected for the double layer effect. The correlation between kinetic and thermodynamic parameters for the charge transfer process and dynamic solvent properties were examined.

Results and Discussion

The process of Ni(Cp)$_2$ electrooxidation was studied using 25 µm radius hemispherical mercury (Au/Hg (25 µm)) and 12.5 µm radius platinum disk (Pt (12.5 µm)) ultramicroelectrodes by ac- and steady-state voltammetry. From the limiting steady-state current the diffusion coefficient of Ni(Cp)$_2$ in different solvents was calculated. The kinetic parameters k_s and α obtained on the basis of admittance-potential curve analysis at a mercury electrode were corrected for the double layer effect. The values obtained for the diffusion coefficients and the observed and corrected kinetic parameters are summarized in Table 1. A good linear relationship between D and the reciprocal of the solvent viscosity has been found (Fig. 1). On the basis of the *Stokes-Einstein* equation, a radius for the reactant ($r_{\mathrm{Ni}(Cp)_2}$) equal to 0.37 nm was calculated. The standard rate constant obtained at a Pt electrode for the $\mathrm{Ni}(Cp)_2^{o/+}$ system can be compared with k_s values reported earlier for the $\mathrm{Fe}(Cp)_2^{o/+}$ system [19]. If we neglect the double layer correction and assume that all processes are adiabatic, the ratio of rate constants should be expressed by Eq. (11).

$$\ln\frac{k_s^{\mathrm{Fe}(Cp)_2}}{k_s^{\mathrm{Ni}(Cp)_2}} = \frac{\Delta G^*_{\mathrm{is,Ni}(Cp)_2} - \Delta G^*_{\mathrm{is,Fe}(Cp)_2} + \Delta G^*_{\mathrm{os,Ni}(Cp)_2} - \Delta G^*_{\mathrm{os,Fe}(Cp)_2}}{\mathrm{RT}} + \frac{1}{2}\ln\frac{\Delta G^*_{\mathrm{os,Fe}(Cp)_2}}{\Delta G^*_{\mathrm{os,Ni}(Cp)_2}} \tag{11}$$

For reactants with similar size, the outer-sphere *Gibbs* reorganisation energies are approximately the same. Therefore, the $\Delta G^*_{\mathrm{os,Ni}(Cp)_2} - \Delta G^*_{\mathrm{os,Fe}(Cp)_2}$ term in Eq. (11) and the logarithmic term of the right hand side of this equation can be neglected. A linear relationship between $k_s^{\mathrm{Fe}(Cp)_2}$ and $k_s^{\mathrm{Ni}(Cp)_2}$ with a slope equal to $\exp((\Delta G^*_{\mathrm{is,Ni}(Cp)_2} - \Delta G^*_{\mathrm{is,Fe}(Cp)_2})/\mathrm{R}T)$ can be expected. The linear dependence of $k_s^{\mathrm{Fe}(Cp)_2}$ on $k_s^{\mathrm{Ni}(Cp)_2}$ is indeed observed (Fig. 2); the slope of this curve, however, which is equal to about 1.2, is much lower than expected based on the difference in

Table 1. Diffusion coefficients, charge transfer coefficients, observed and corrected standard rate constants, and experimental activation enthalpies of the $\mathrm{Ni}(Cp)_2^{o/+}$ system

Solvent	D (10^5 cm^2/s)	Au/Hg (25 µm)			Pt (12.5 µm)		
		α	$k_s^{(obs)}$ (cm/s)	$k_s^{(corr)}$ (cm/s)	α	$k_s^{(obs)}$ (cm/s)	ΔH^*_{ex} (kJ/mol)
ACN	1.62	0.54	0.71	4.0	0.47	2.0	18.4
AC	1.85	0.53	0.55	4.2	0.51	1.8	17.1
BN	0.95				0.49	0.52	20.5
DCM	1.25	0.50	0.40	4.5	0.50	1.4	18.4
DMF	0.71	0.51	0.14	1.45	0.52	0.54	23.1
DCE	0.75	0.47	0.25	3.0	0.51	0.80	18.8
DMSO	0.35	0.51	0.10	0.92	0.52	0.20	26.3
PC	0.30	0.51	0.055	0.42	0.49	0.12	30.1

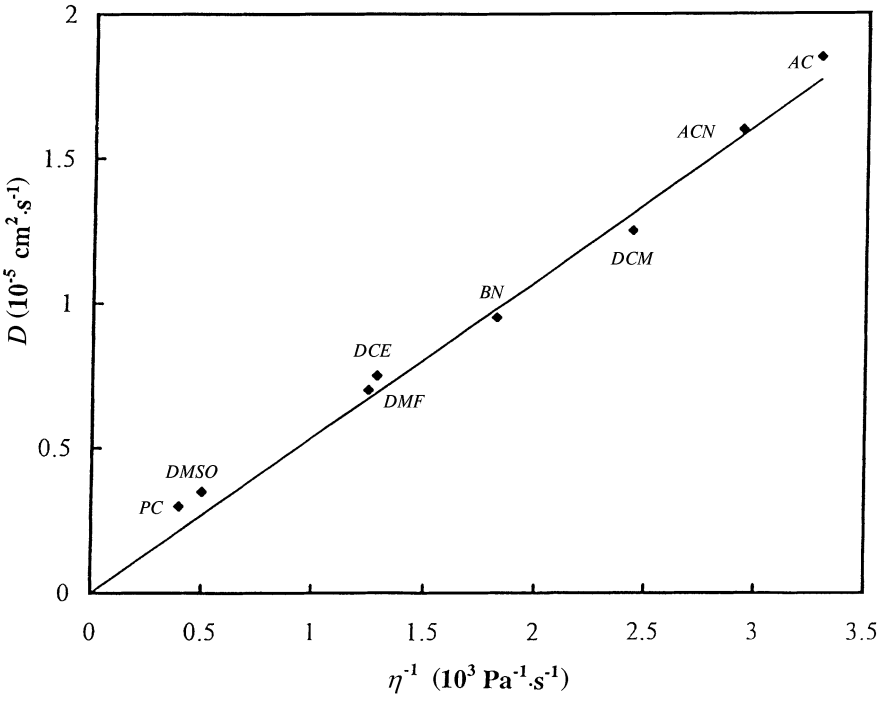

Fig. 1. Diffusion coefficient of Ni(Cp)$_2$ in various solvents plotted against reciprocal viscosity; background electrolyte: 0.1 *M TBAP*

the inner-sphere reorganization energies. Inner-sphere *Gibbs* reorganization energies of 0.6 kJ/mol and 2.7 kJ/mol have been calculated for the Fe$(Cp)_2^{o/+}$ [18] Ni$(Cp)_2^{o/+}$ [29] systems, respectively. Based on these values, the slope of the curve presented in Fig. 2 should be close to 2.3. The different potential ranges of nickelocene and ferrocene oxidation and, therefore, the different magnitude of double layer correction may explain the observed disagreement. Further, the electrode processes at a platinum electrode may be modified by traces of some organic compounds present in the organic solvents. Organic impurities are likely to be chemisorbed on the platinum, thereby affecting its response. It has been suggested [28] that the adsorption of organic impurities on Pt is responsible for the independence of the rate of ferrocene oxidation on the outer-*Helmholtz* plane potential [28].

The $\ln k_s - \ln \tau_L$ and $\ln k_s - \ln \eta$ correlation

The dependences of the logarithm of the rate constant on the logarithm of relaxation time and viscosity are presented in Fig. 3. In both cases, a rather week correlation is observed. Correlation coefficients equal to 0.851 and 0.855 were found for the $\ln k_s - \ln \tau_L$ relation obtained at Au/Hg (25 μm) and Pt (12.5 μm) electrodes, respectively. A slightly better correlation is found between the logarithm of the standard rate constant and the logarithm of solvent viscosity (correlation coefficients 0.959 and 0.937 for Au/Hg (25 μm) and Pt (12.5 μm)

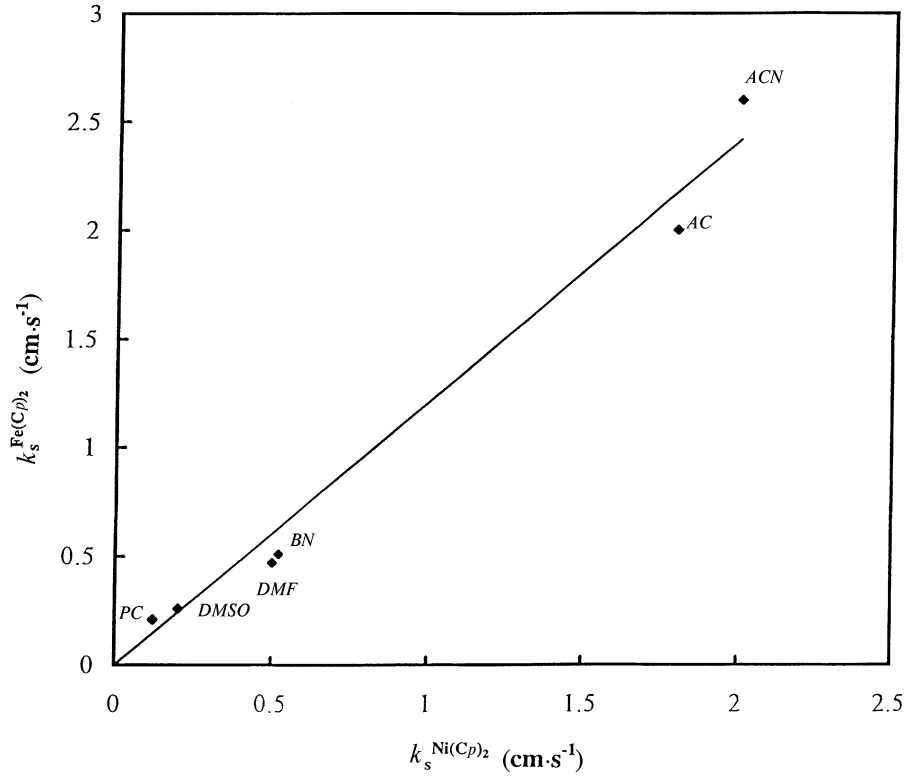

Fig. 2. Plot of the formal rate constant of ferrocene electrooxidation against the formal rate constant of nickelocene electrooxidation at a platinum electrode

electrodes). From the slopes of these plots, Θ parameters equal to 0.9 and 1.1 were found for the $\ln k_s - \ln \tau_L$ and $\ln k_s - \ln \eta$ functions, respectively. A value of Θ close to 1 suggests adiabacity for the studied process.

The relations between $ln\,(k_s/(\Delta G^*_{os})^{1/2}) + \Delta G^*_{os}/RT$ *and* $ln\,\tau_L$ *or* $ln\,\eta$

This approach accounts for both the effect of solvent dynamics and the effect of outer-sphere reorganization energy on the rate of electron transfer. In this case, the values of ΔG^*_{os} calculated according to *Marcus* and the MSA model were considered. It was also assumed that the image effect can be neglected. For the corrected standard rate constant values obtained at a mercury electrode, a good linear correlation between $\ln\,(k_s/(\Delta G^*_{os})^{1/2}) + \Delta G^*_{os}/RT$ and $\ln \tau_L$ was observed regardless of the model used for the outer-sphere activation energy calculation (Fig. 4a). The slopes of both straight lines are slightly higher than unity (-1.18 ± 0.08). In Fig. 4a, the broken straight lines were obtained by forcing the slope to be equal to unity. The same analysis performed using the observed values for the standard rate constants obtained at a Pt (12.5 μm) electrode also shows a straight line, but the slope is much higher (-1.44 ± 0.12). The correlation coefficient obtained for the observed k_s values is lower than that obtained for corrected standard rate constants. A comparison of Figs. 3a and 4a points out

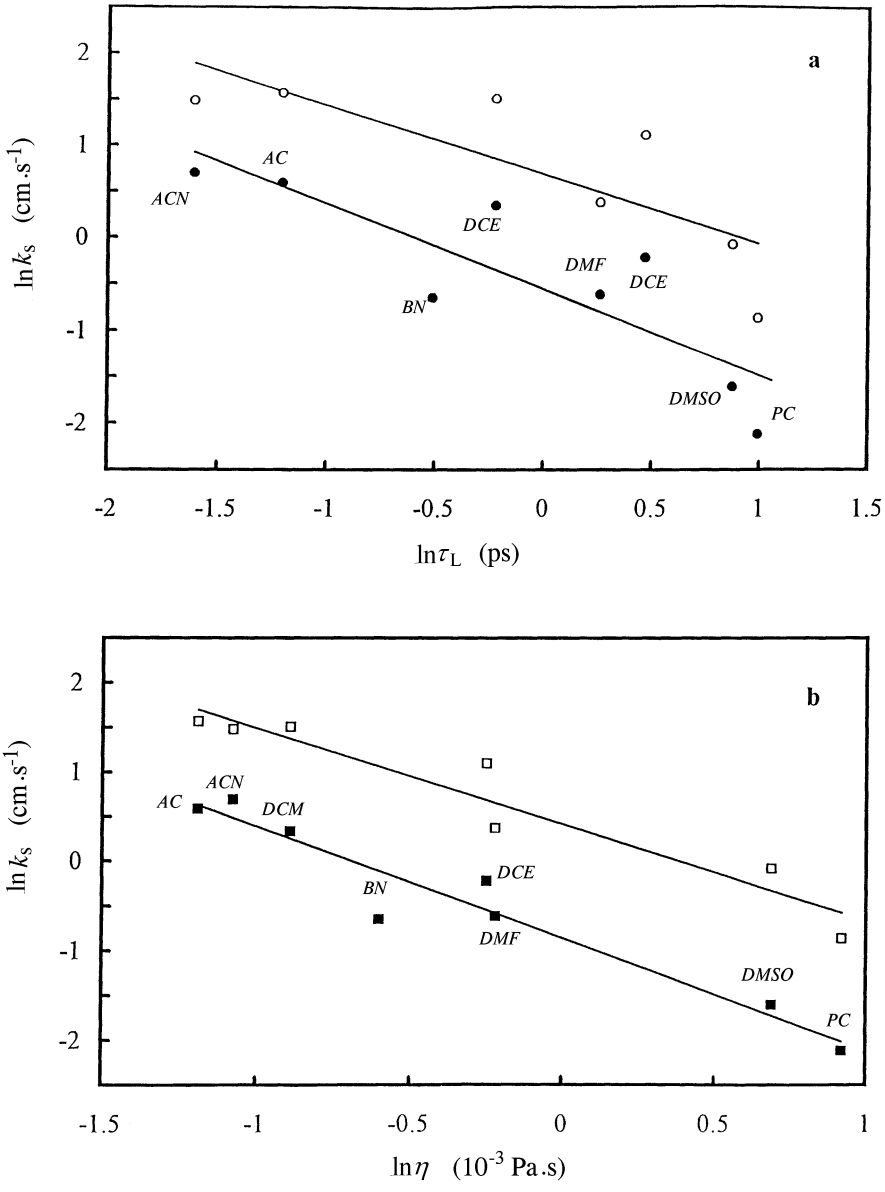

Fig. 3. Plots of the logarithm of the corrected (empty markers) and observed (filled markers) formal rate constants for the electrooxidation of Ni(Cp)$_2$ against the logarithm of the longitudinal relaxation time (a) and the logarithm of the solvent viscosity (b); corrected rate constants: Au/Hg (25 μm), observed rate constants: Pt (12.5 μm) ultramicroelectrode

that the correlation between $\ln(k_s/(\Delta G^*_{os})^{1/2}) + \Delta G^*_{os}/RT$ and $\ln \tau_L$ is much better than the simple $\ln k_s - \ln \tau_L$ correlation frequently used in the analysis of kinetic data of fast electrode reactions. From the intercept of the linear relations presented in Fig. 4a, the κK_p parameter can be calculated. However, even small errors in the determination of the slope may significantly change the intercept. In order to reduce this effect, the κK_p parameter was calculated from the intercept of straight lines obtained by forcing the slope equal to 1. A value of κK_p equal to

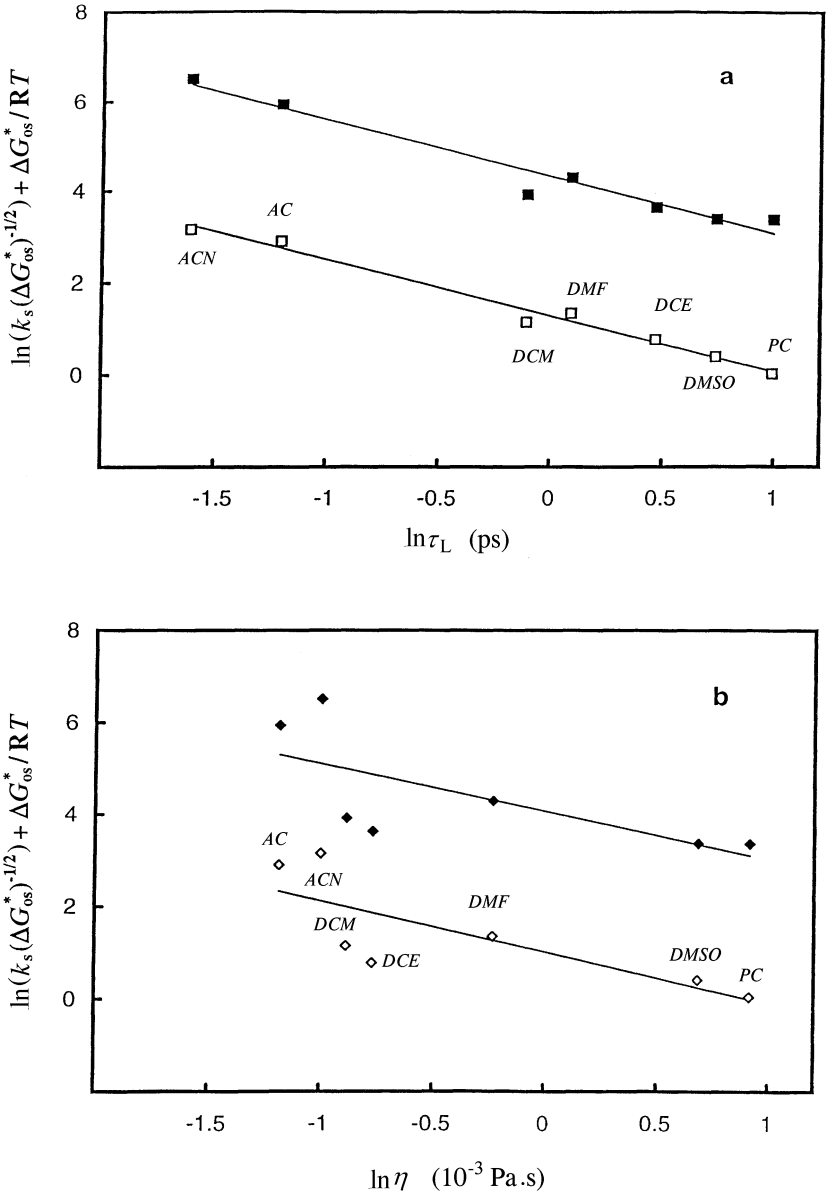

Fig. 4. Plots of $\ln(k_s/(\Delta G^*_{os})^{1/2}) + \Delta G^*_{os}/RT$ for the electrooxidation of Ni(*Cp*)$_2$ at Au/Hg (25 µm) against the logarithm of the longitudinal relaxation time (a) and the logarithm of the solvent viscosity (b); ΔG^*_{os} was calculated according to *Born* (filled markers) and MSA (empty markers) models

20 ± 12.5 pm was obtained using the corrected values for the standard rate constants and ΔG^*_{os} calculated according to the MSA model. This value is only slightly lower than that predicted by *Hupp* and *Weaver* [30]. For ΔG^*_{os} calculated according to *Marcus*, the κK_p parameter is much higher then the value predicted by *Hupp* and *Weaver* [30].

A completely different situation was observed if the $\ln(k_s/(\Delta G^*_{os})^{1/2}) + \Delta G^*_{os}/RT$ term was correlated with the logarithm of solvent viscosity. A very poor correlation with almost random error was found in this case (Fig. 4b).

The correlation between ΔH^*_{ex} and ΔH_L or ΔH_D

This analysis refers to Eqs. (7) and (8) and assumes that the change of longitudinal relaxation time is the predominant factor in the solvent effect. In this case, a linear correlation between the experimentally obtained activation enthalpy $\left(\Delta H^*_{\mathrm{ex}}\right)$ minus the estimate of ΔH^*_{os} and longitudinal relaxation enthalpy (ΔH_{L}) should be observed. The plot of $\Delta H^*_{\mathrm{ex}} - \Delta H^*_{\mathrm{os}}$ *vs.* ΔH_{L} is presented in Fig. 5a. The higher scatter reflects the relatively large error involved in determining the experimental activation enthalpy. From the slope of this relation, a Θ parameter equal to 0.98 ± 0.13 was calculated. From the intercept, an inner-sphere activation energy of $1.75\,\mathrm{kJ \cdot mol^{-1}}$ was calculated. This value is close to the value calculated according to the harmonic oscillator model [29].

$$p' = \frac{D}{2\,D_{\mathrm{r}}\sigma} \tag{12}$$

According to the transitional model of the adiabatic electron transfer process [31], the pre-exponential factor depends on the p' parameter defined by Eq. (12) where D is the translational diffusion coefficient, D_{r} is the rotational diffusion coefficient, and σ is the diameter of the solvent molecule. If one neglects the changes in D_{r} with temperature, a linear relation between $\Delta H^*_{\mathrm{ex}} - \Delta H^*_{\mathrm{os}}$ and ΔH_{D} can be expected. This correlation is presented in Fig. 5b. The values of diffusion enthalpies were obtained from the slope of $\ln D$ *vs.* $1/T$. relations. From the slope of the straight line presented in Fig. 5b, a Θ parameter equal to 1.25 ± 0.08 was calculated. The intercept of the straight line presented in Fig. 5b is almost equal to 0.

It is observed that the $\Delta H^*_{\mathrm{ex}} - \Delta H^*_{\mathrm{os}}$ difference correlates well both with the ΔH_{L} and ΔH_{D} enthalpies. However, the intercept and slope of the correlation between experimental enthalpy and longitudinal relaxation enthalpy are much closer to the values predicted by theory.

The comparison of experimental and theoretical values of Gibbs' activation energy

The theoretical values of *Gibbs*' activation energy were calculated on the basis of *Marcus* and MSA models neglecting the image effect. In order to calculate the outer-sphere enthalpy of activation, the corresponding entropy was estimated by differentiation of Eq. (2) with respect to temperature [17]. Values of ΔG^*_{os} and ΔH^*_{os} calculated according to both the *Born* and MSA models are summarized in Table 2. According to Eqs. (7) and (8), the experimental values of the activation enthalpy $(\Delta H^*_{\mathrm{os}})$ can be estimated on the basis of the following relationships:

$$\Delta H^*_{\mathrm{os}} = \Delta H^*_{\mathrm{ex}} - \Delta H^*_{\mathrm{is}} - \Delta H_{\mathrm{L}} \tag{13}$$

$$\Delta H^*_{\mathrm{os}} = \Delta H^*_{\mathrm{ex}} - \Delta H^*_{\mathrm{is}} - \Delta H_{\mathrm{D}} \tag{14}$$

The theoretical and experimental values of the activation enthalpy are also summarized in Table 2. These data demonstrate that the activation enthalpies calculated according to the *Born* model are too high in comparison to the experimental data. However, there is a very good agreement between the experimental ΔH^*_{os} values calculated according to Eq. (13) and theoretical results

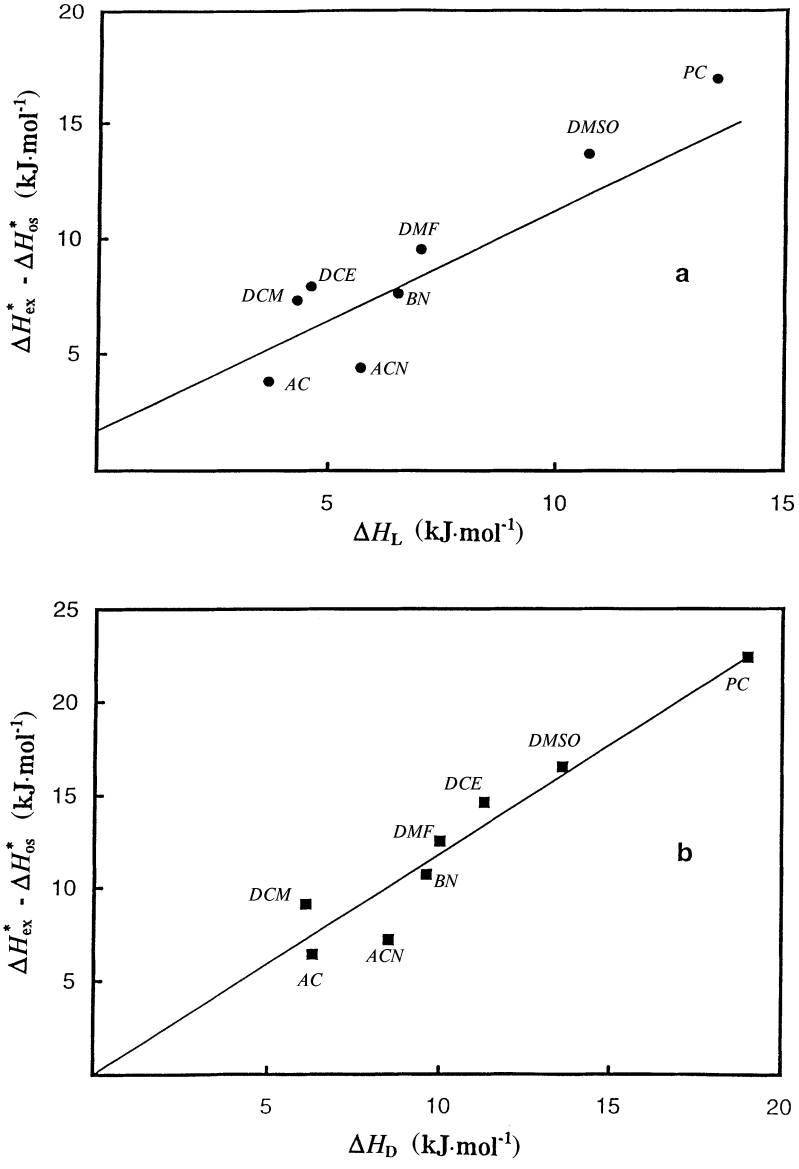

Fig. 5. Plots of the difference between the experimental activation enthalpy ΔH^*_{ex} and the MSA estimate of the outer-sphere contribution, ΔH^*_{os}, for Ni$(Cp)_2^{o/+}$ against the activation enthalpy for longitudinal relaxation (ΔH_L, a) and diffusion (ΔH_D, b)

calculated on the basis of the MSA model. The values of ΔH^*_{os} calculated according to Eq. (14) are significantly smaller than those predicted by the MSA model.

On the basis of the experimental values for the outer-sphere reorganization energy and the corrected standard rate constants, the κK_p parameters were calculated for different solvents. The pre-exponential factor was calculated assuming dependence of the electron transfer kinetics on the longitudinal relaxation time (Eq. (1)) and on both longitudinal and rotational relaxation times

Table 2. Comparison of estimated and experimental values of outer-sphere reorganization energy ($kJ \cdot mol^{-1}$)

Solvent	ΔG^*_{os} (*Born*)	ΔG^*_{os} (*MSA*)	ΔH^*_{os} (*Born*)	ΔH^*_{os} (*MSA*)	ΔH^{*a}_{os}	ΔH^{*b}_{os}
ACN	24.8	16.1	21.2	14.7	14.0	11.2
AC	23.2	15.3	20.8	14.1	13.3	10.7
BN	22.4	14.2	20.3	13.9	12.9	9.8
DCM	17.8	10.4			11.1	9.3
DMF	21.7	14.0	19.2	13.1	13.6	10.6
DCE	18.1	10.5			10.9	4.2
DMSO	20.5	12.7	18.1	12.3	12.7	9.8
PC	22.5	13.8	19.7	13.2	13.2	7.7

[a] Calculated according to Eq. (13); [b] calculated according to Eq. (14)

Table 3. Values of the κK_p parameter calculated for corrected rate constants and different reorganization energies

Solvent	κK_p (pm) for ΔG^*_{os} (*Born*)	for ΔG^*_{os} (*MSA*)	for ΔH^{*a}_{os}	for ΔH^{*b}_{os}
ACN	714	25	12	4
	3400[c]	98[c]	42[c]	14[c]
AC	603	29	14	5
	3100[c]	125[c]	55[c]	19[c]
DCM	241	16	20	10
	431[c]	24*c*	30[c]	15[c]
DMF	426	23	19	6
	2100[c]	98[c]	84[c]	26[c]
DCE	320	19	22	2
DMSO	325	17	17	6
	392[c]	19[c]	19[c]	6[c]
PC	413	15	12	2

[a] Obtained on the basis of Eq. (12); [b] obtained on the basis of Eq. (13); [c] calculated assuming that the pre-exponential factor is expressed by Eq. (6)

(Eq. (6)). Additionally, the κK_p parameters were calculated for theoretical values of the activation energy estimated on the base of *Born* and MSA models. The values for the κK_p parameter obtained for different solvents are collected in Table 3. A significant increase in κK_p is observed when the internal effect on the pre-exponential factor is considered, particularly for solvents with very low longitudinal relaxation time.

Conclusions

(*i*) The correlation between kinetic data obtained for the processes of nickelocene and ferrocene oxidation indicates that the influence of the double layer structure on the electrode kinetics of metalloocene oxidation is significant and has to be considered in the solvent effect interpretation.

(*ii*) The solvent effect on the charge transfer process in $Ni(Cp)_2^{o/+}$ system can be successfully described on the basis of the encounter-pre-equilibrium model. The electron transfer barrier height and the solvent dynamics are the most important factors contributing to the measured rate constants of nickelocene electrooxidation.

(*iii*) The Θ parameter of this redox process is close to 1, indicating adiabacity of electron transfer process.

(*iv*) A better agreement between theoretical prediction and experimental results is obtained when the kinetic data of $Ni(Cp)_2$ oxidation are correlated with the longitudinal relaxation time (τ_L) and relaxation activation enthalpy (ΔH_L) than in the case of correlation between the kinetic data and viscosity of the solvent (η) and diffusion enthalpy (ΔH_D).

(*v*) The comparison of theoretical and experimental values of activation energies indicates that the MSA model is much better at describing the solvation phenomena than the classical *Born* model.

(*vi*) For solvents with low longitudinal relaxation time, the rotational relaxation time has to be considered in the analysis of the solvent effect on the kinetics of the charge transfer process.

Experimental

All solvents are analytical grade. Dimethylformamide (*DMF*), acetonitrile (*ACN*), dichloromethane (*DCM*), 1,2-dichloroethane (*DCE*), butyronitrile (*BN*), propylene carbonate (*PC*), acetone (*AC*), and dimethylsulfoxide (*DMSO*) were dried over calcium hydride for one day and then distilled under vacuum. Tetrabutylammonium perchlorate (*TBA*ClO_4) was precipitated from an aqueous solution of tetrabutylammonium hydroxide (Aldrich) with perchloric acid, washed with water and dried under vacuum. Triply distilled mercury (Fisher) was purified further in order to remove any metals by the procedure suggested in the polarographic analyzer manual (EG&E Princeton Applied Research). Nickelocene (Aldrich) was used without further purification.

All electrochemical measurements were performed using a Ag/0.1 *M* $AgNO_3$ in *ACN* reference electrode. The reference electrode solution was separated from the analyzed solution by 3 Å molecular sieves (BDH Chemicals). The silver solution was replaced daily because of the instability of Ag^+ to photoreduction in the solvent. The counter electrode was made of platinum foil. Ultramicroelectrodes were manufactured by sealing a metal wire (Goodfellow Metals Ltd. UK) into a soft glass capillary by means of a *Bunsen* flame. The capillary was then cut perpendicularly to its length, and the surface was polished using extra fine carborundum paper followed by 0.3 μm alumina. Electrical contacts were made using silver epoxy (Johnson Mattey Ltd. UK). The hemispherical mercury electrode was prepared by electrodeposition of the proper amount of mercury from an aqueous solution of 1 *M* $Hg_2(ClO_4)_2$ in $HClO_4$ onto a polished Au disk electrode. The mercury deposition time was computer controlled. In the study of double layer capacity and in the determination of standard potentials and diffusion coefficients, a hanging mercury drop electrode (HMDE) with a surface area of 0.0094 cm^2 was used. All solutions were deaerated for 20 min with argon prior to the electrochemical measurements.

In dc- and ac-voltammetric experiments, an EG&E Princeton Applied Research (PAR) Model 273 and a PC 6300 AT&T computer were used. In dc-voltammetric measurements, a positive feedback *iR* compensation was employed. The admittance potential data were obtained for different frequency values in the potential range of faradaic processes. The background in-phase and out-of-phase admittances were fitted before and after the peak of the faradaic process into a third order polynomial expression by the least squares method, and the background admittances under the peak

were numerically evaluated. The solution resistance and double layer capacitance were found from the background in-phase and out-of-phase admittance at the faradaic process potential. Admittance data obtained as a function of potential were analyzed according to the method of *Levie* and *Husovsky* [32]. The optimum frequency range was obtained from a simulation program [27]. The ac-voltammetric experiments on HMDE were carried out in order to determine the double layer capacity of the Hg electrode in the studied solutions. Potentials of zero charge (E_{zc}) were obtained polarographically from the zero charge current (*DCM*, *DMF*, *DCE*, *DMSO*, and *PC*) or from the minimum of differential capacity in solutions containing low concentrations of the supporting electrolyte (*ACN* and *AC*). The classical *Frumkin* correction of kinetic parameters for double layer effects [33] was performed.

Constant temperatures down to −55°C were obtained using a methanol bath in a *Dewar* flask whose temperature was controlled with an immersion cooler.

Acknowledgements

The author thanks Prof. *A. S. Baranski* and Prof. *W. R. Fawcett* for valuable help and discussion.

References

[1] Fawcett WR (1989) Langmuir **5**: 661
[2] Fawcett WR, Opallo M (1994) Angew Chem Int Ed Engl **33**: 2131
[3] Weaver MJ (1992) Chem Rev **92**: 463
[4] Weaver MJ (1992) In: Guidelli R (ed) Electrified Interfaces in Physics, Chemistry and Biology. Kluwer, Dordrecht pp 427–442
[5] Blum L, Fawcett WR (1991) Chem Phys Lett **187**: 173
[6] Calef DF, Wolynes P (1983) J Phys Chem **87**: 3387
[7] Calef DF, Wolynes P (1983) J Chem Phys **78**: 470
[8] Fawcett WR, Kovacova Z (1990) J Electroanal Chem **292**: 9
[9] Gennett T, Milner DF, Weaver MJ (1985) J Phys Chem **89**: 2787
[10] McManis GE, Golvin MN, Weaver MJ (1986) J Phys Chem **90**: 6563
[11] Phelps DK, Ramm MT, Wang Y, Nelson SF, Weaver MJ (1993) J Phys Chem **97**: 181
[12] Opallo M, Kapturkiewicz A (1985) Electrochim Acta **30**: 1301
[13] Opallo M (1986) J Chem Soc Faraday Trans 1, **82**: 339
[14] Kapturkiewicz A, Jaenicke W (1987) J Chem Soc Faraday Trans 1, **83**: 2727
[15] Grampp G, Kapturkiewicz A, Jaenicke W (1990) Ber Bunsenges Phys Chem **94**: 1343
[16] Fawcett WR, Opallo M (1992) J Electroanal Chem **331**: 815
[17] Fawcett WR, Opallo M (1992) J Phys Chem **96**: 2920
[18] Baranski AS, Winkler K, Fawcett WR (1991) J Electroanal Chem **313**: 367
[19] Fawcett WR, Fedurco M (1993) J Phys Chem **97**: 7075
[20] Harrer W, Grampp G, Jaenicke W (1986) J Electroanal Chem **209**: 223
[21] Kapturkiewicz A, Behr B (1984) J Electroanal Chem **179**: 187
[22] Zhang X, Leddy J, Bard AJ (1985) J Am Chem Soc **107**: 3719
[23] Davies M (1969) In: Hill NE, Vaughan WE, Price AH, Davis M (eds) Dielectric Properties and Molecular Behavior. Van Nostrands Reinhold, London, chapter 5
[24] Fawcett WR, Foss CA Jr (1988) J Electroanal Chem **252**: 221
[25] Fawcett WR, Foss CA Jr (1989) J Electroanal Chem **270**: 103
[26] Grampp G, Jaenicke W (1991) Ber Bunsenges Phys Chem **95**: 904
[27] Baranski AS (1991) J Electroanal Chem **300**: 309
[28] Winkler K, Baranski AS (1993) J Electroanal Chem **346**: 197

[29] Winkler K, Baranski AS, Fawcett WR (1996) J Chem Soc Faraday Trans **92**: 3899
[30] Hupp JT, Weaver MJ (1984) J Phys Chem **98**: 1463
[31] Baghi B, Chandra A, Fleming GR (1990) J Phys Chem **94**: 5197
[32] de Levie R, Husovsky AA (1969) J Electroanal Chem **22**: 29
[33] Bard AJ, Faukner LR (1980) Electrochemical Methods Fundamentals and Applications. Wiley, New York, pp 550–554

Received February 6, 1998. Accepted (revised) April 24, 1998